Determining the Ratio of the Gaussian Curvature and Bending Elastic Moduli of Phospholipids from Q_{II} Phase Unit Cell Dimensions

David P. Siegel
Givaudan, Inc., Cincinnati, Ohio

ABSTRACT A method is presented for measuring M, the ratio of the Gaussian (saddle splay) elastic modulus to the bending elastic modulus of a lipid monolayer. The ratio M is determined from measurements of the equilibrium bicontinuous inverted cubic (Q_{II}) phase unit cell size in excess water as a function of temperature. The analysis includes the effect of a curvature elastic term that is second-order in the Gaussian curvature, K. Preliminary results using data on DOPE-Me validate the method. The fitted value of M is within 8% of the value estimated in an earlier treatment. The method can be used to measure changes in M due to addition of exogenous lipids and peptides to a host lipid system. The Gaussian elastic modulus has a substantial effect on the stability of fusion intermediates (stalks, hemifusion diaphragms, and fusion pores). Studying the effects of peptides and different lipids on M via this method may yield insights into how fusion protein moieties stabilize intermediates in membrane fusion in vivo. The contribution of the K^2 curvature elastic term to the free energy of Q_{II} phase and fusion pores explains some features of fusion pore stability and dynamics, and some peculiar observations concerning the mechanism of L_α/Q_{II} phase transitions.

INTRODUCTION

The stability of Q_{II} phases versus the L_α phase is determined by the Gaussian (saddle splay) modulus of the lipid bilayers, which can be expressed in terms of the lipid monolayer elastic properties (1–4); the spontaneous curvature (splay) J_s, the bending modulus, k_m, and the Gaussian (saddle splay) elastic modulus, κ, of the monolayers. One can estimate the ratio of the monolayer Gaussian and bending elastic moduli by measuring J_s as a function of temperature and the L_α/Q_{II} phase transition temperature, T_Q (4). However, L_α/Q_{II} transitions in phospholipids are very hysteretic (e.g., (5)), and it can be hard to measure T_Q. It is difficult to know whether or not one is observing an effect of the additive on the transition kinetics (i.e., on the hysteresis), or on the equilibrium transition temperature. One can measure k_m and J_s by appropriate experiments on the equilibrium lattice constants of H_{II} phases (6). Thus, one can measure small changes in k_m and J_s made by addition of different lipids and peptides, to infer their effects on a process like biomembrane fusion. Ideally, one would like to do the same sort of experiment on Q_{II} phases to measure κ, for the same reasons.

However, the free energy of the Q_{II} versus the L_α phase is a more complicated function than that for the H_{II} phase (7). In addition to the Gaussian curvature energy contribution, the contribution of chain-packing energies is more complicated than in the case of the H_{II} phase (8). In addition, the expression for the curvature energy of the monolayers must include terms that are third- or fourth-order in monolayer curvature, rather than only the second-order terms used in the standard Helfrich treatment (1). This is especially true in systems with small Q_{II} phase-unit cell constants (c) of ~10 nm, like the monoglycerides (9). This makes analysis of the Q_{II} phase-unit cell constant, in terms of the elastic parameters, more complicated than for the H_{II} phase.

However, on the basis of recent theoretical work (3), it is clear that the contributions of chain-packing terms should be negligible for Q_{II} phases cells with large c-values like those found in phospholipids near T_Q (20–40 nm (4,10)). Moreover, for systems with large values of c, the contributions of higher-order curvature terms are much smaller than for systems with smaller c, and the mathematical expressions are more tractable. For example, a series expression for a term involving the area-averaged value of the square of the Gaussian curvature in a Q_{II} phase (8) requires four terms in higher-order curvature integrals to be accurate to within 5% for $c = 6$ nm, but only the first term to achieve the same accuracy for $c \geq 17$ nm. Nevertheless, the higher-order terms in the expression for the Q_{II} phase curvature energy still play an important role, especially the term in the square of the Gaussian curvature. This term imposes an equilibrium value of c. A previous model for the free energy of the Q_{II} phase (4), using only the first-order term in the Gaussian curvature, predicts indefinite shrinkage of c (4). It would be helpful to estimate the size of the higher-order terms, to gain further insights into the factors underlying Q_{II} phase stability, and into the influence of these terms on fusion pore dynamics (discussed below).

In the present treatment, contributions to the curvature energy that are third- and fourth-order in monolayer curvature are used. An expression is derived for the equilibrium value of the Q_{II} phase-unit cell constant in excess water, c_{eq}, as a function of J_s (which is a function of the temperature). By fits to plots of c_{eq} versus a function of J_s, one can determine the ratio of the Gaussian and bending elastic moduli of the system, as well as measure the coefficients of the term that is second-order in Gaussian curvature. Analysis

Submitted March 16, 2006, and accepted for publication April 18, 2006.

Address reprint requests to D. P. Siegel, E-mail: david.siegel@givaudan.com.

0006-3495/06/07/608/11 $2.00

doi: 10.1529/biophysj.106.085225

of the c_{eq} data for DOPE-Me in Cherezov et al. (5) and comparison with an earlier estimate by Siegel and Kozlov (4) validates the treatment.

The results have two important implications. First, the method can be used to determine the effects of exogenous lipids and peptides on κ. The value κ has a substantial influence on the curvature energy of intermediates in membrane fusion (4,11), and of topologically complicated membrane structures in organelles (12). The exact mode of action of moieties of fusion-modulating proteins in catalyzing fusion is still not clear. It has been proposed that these moieties (e.g., fusion peptides, transmembrane peptides) act in part by changing κ (13,14), and the present method offers a way to test this hypothesis. Second, as shown in this article, the higher-order Gaussian curvature terms influence the energies and equilibrium dimensions of fusion pores. Fusion pores are intermediates in L_α/Q_{II} phase transitions (4,5,13). It is shown that there is essentially no driving force for opening of nascent fusion pores in tension-free membranes beyond a water channel radius of 2–4 nm. This may be relevant to the function of viral fusion proteins: it is now clear that one function of these proteins is to ensure that nascent fusion-pores open to sizes where they cannot easily revert to earlier intermediates in the fusion process (see (15) for a review).

Finally, the predicted dimensions of fusion pores in multilamellar arrays have implications for the mechanism of the L_α/Q_{II} phase transition. The results may explain the curious tendency of the unit cell size of some nascent Q_{II} phases in phospholipids to decrease with time at constant temperature after formation in the presence of excess water.

THEORY

The curvature free energy of the Q_{II} phase with respect to the L_α phase is solely due to the Gaussian curvature elastic energy of the bilayer (4). As in Siegel and Kozlov (4), we neglect terms arising from monolayer thickness variations across the unit cell, since these terms are negligible for the relevant range of c (3). Our approach is to write the expression for the curvature free energy of the bilayer in a Q_{II} phase in terms of the free energy of the constituent monolayers. Unlike the treatment in Siegel and Kozlov (4), we include terms that are third- and fourth-order in monolayer curvature. As shown in Appendix A (Eq. A17), this results in an expression for the free energy per unit area of bilayer (f_B) of the Q_{II} phase in terms of powers of the area-averaged Gaussian curvature evaluated at the bilayer midplanes. To second-order in Gaussian curvature, this expression is

$$f_B = \kappa_1\left[\frac{S_1}{S_0}\right]\left(\frac{1}{c^2}\right) + \kappa_2\left[\frac{S_2}{S_0}\right]\left(\frac{1}{c^4}\right), \quad (1)$$

where

$$\kappa_1 = (2\kappa - 4\delta k_m J_s + \delta^2 k_m J_s^2), \quad (2)$$

$$S_N = c^{2N-2}\int_{Q-phase} K^N dA, \quad (3)$$

where N is the subscript of the dimensionless coefficient, S_N. The value δ is the distance between the bilayer midplanes and the neutral surface of the lipid monolayers. The value δ can be estimated from x-ray diffraction experiments, and is 1.3 nm for oleoyl-chain lipids (4). The value K is the Gaussian curvature of the bilayer midplanes. The value c is the unit-cell constant of the Q_{II} phase (the length of one side of the unit cell). The coefficients S_N have different values for the Q_{II} phases corresponding to different infinite periodic minimal surfaces (*Im3m*, *Pn3m*, and *Ia3d*; based on the P, D, and G surfaces of Schoen (16)). The values of S_N up to $N = 8$ have been tabulated for *Pn3m* (3,8), and a method for calculating them for the other Q_{II} phases from the values for *Pn3m* is given in Schwarz and Gompper (3). Values for the three commonly-observed bicontinuous Q_{II} phases are given in Table 1. Note that the values for *Pn3m* in Schwarz and Gompper (3) are for a unit cell twice as large as for the values in Anderson et al. (8). The values in Anderson et al. (8) and Table 1 are appropriate for analysis of x-ray data from Q_{II} phases composed of bilayers without sidedness.

Note that S_1 is always < 0, and S_0 and S_2 are > 0. The first term on the right-hand side of Eq. 1 provides the driving force for Q_{II} phase formation. The value f_B is <0 (Q_{II} phase can form spontaneously) when $\kappa_1 > 0$ (Eq. 2). The value κ_1 is <0 at low temperatures, and increases with increasing temperature, because J_s increases (becomes less negative) with increasing temperature. (The temperature dependence of J_s can be thought of as arising from the increase in conformational freedom of the acyl chains of the lipids with increasing temperature. Crudely, this tends to make the lipids more cone-shaped, increasing the relative cross-sectional area of the lipid moieties relative to the headgroup area.) Let T_K be the temperature at which $\kappa_1 = 0$; this corresponds to the temperature above which there will be a driving force for formation of structures with $K < 0$, like Q_{II} phases. Because of the positive second term on the right-hand side of Eq. 1, formation of Q_{II} phases will not become spontaneous until a slightly higher temperature (T_Q) is reached, depending on the value of c.

By differentiating Eq. 1 with respect to c, setting the result equal to zero to establish the condition for mechanical equilibrium, and rearranging, one obtains an expression for the equilibrium unit cell constant in excess water, c_{eq} (Eq. A18). For purposes of fitting Eq. A8 to the data, it is convenient to express κ_1 as

$$\kappa_1 = 2k_m(M - x), \quad (4)$$

where

$$M = \frac{\kappa}{k_m} \quad (5)$$

and

$$x = 2\delta J_s - \frac{\delta^2}{2}J_s^2. \quad (6)$$

Then one can express Eq. A18 as

TABLE 1 Values of S_N for different Q_{II} phases

Coefficient	D (*Pn3m*)*	P (*Im3m*)	G (*Ia3d*)
S_0	1.91889	2.34510	3.09144
S_1	-4π	-8π	-16π
S_2	100.294	328.270	996.071
S_3	−865.936	$-4.638.34 \times 10^3$	-2.13526×10^4
S_4	7.82252×10^3	6.85733×10^4	4.78930×10^5
S_5	-7.28926×10^4	-1.04583×10^6	-1.10818×10^7

In the column headings, the designation of the infinite periodic minimal surface according to the nomenclature of Schoen (16) is followed by the space group of the corresponding bicontinuous Q_{II} phase.

*Results from Anderson et al. (8). The coefficients S_2–S_5 were calculated for the other Q_{II} phases using the values for D (*Pn3m*) according to the method given in Schwarz and Gompper (3).

$$c_{eq} = \sqrt{\frac{b}{(M - x)}}, \tag{7}$$

where

$$b = -\frac{\kappa_2}{k_m}\frac{S_2}{S_1}. \tag{8}$$

For a given composition, M and b are determined by fitting Eq. 7 to plots of c_{eq} versus x, where x is a function only of known quantities, i.e., J_s and δ. It is also possible to estimate M if T_K can be estimated experimentally. For example, T_K should be approximately the temperature at which prominent isotropic ^{31}P NMR resonances appear as a function of increasing temperature, indicating formation of numerous fusion pores (4). The value of $\kappa_1 = 0$ at $T = T_K$, so from Eq. 4, M is given by the value of x at $T = T_K$ (Eq. 6). If we know the value of δ and of J_s as a function of temperature, we can estimate M. However, it is more accurate to determine M from a fit of c_{eq} versus x.

In Fig. 1 *A* we plot the expected value of c_{eq} (Eq. A18) against x (Eq. 6) for a DOPE-Me *Pn3m* phase. In Fig. 1 *B* we plot the expected values of c_{eq} versus T with the same assumptions. Initially, the value of c_{eq} decreases rapidly for $T > T_K$ (Fig. 1 *B*). In practice, sample water content and transport considerations will limit c_{eq} at T very close to T_K. The curves in Fig. 1 (*dashed lines*) are calculated with different values of κ_2/k_m. As discussed in Appendix A, the estimated range of κ_2/k_m is $0 < \kappa_2/k_m < 4\delta^2$. We have plotted the curves for this maximum value, and for three intermediate values ($2\delta^2$, δ^2, and $\delta^2/2$). In Fig. 1, *A* and *B*, observed values of c_{eq} for DOPE-Me from Cherezov et al. (5) are also plotted, as data points. The dotted line in Fig. 1 *A* is a fit of the DOPE-Me data to Eq. 7, made with SigmaPlot 8.0 (SPSS, Chicago, IL). The value of κ_2/k_m obtained from the fit in Fig. 1 *A* is used to plot the expected T-dependence of c_{eq} in Fig. 1 *B*.

THEORETICAL RESULTS

Expected dependence of c_{eq} on x and T

To model the dependence of c_{eq} on x, we use values of $J_s(T)$, k_m, and δ for DOPE-Me from Siegel and Kozlov (4), and plot c_{eq} for different assumed values of κ_2/k_m. For these calculations, we use a value of M estimated in a fashion similar to that in Siegel and Kozlov (4).

We assume that the temperature at which Q_{II} phase first appears in DOPE-Me after long incubations is approximately equal to T_K. This temperature is ~55°C (5). The value T_K is the temperature at which $\kappa_1 = 0$. Using the values of J_s at 55°C (5) and $\delta = 1.3$ nm in Eqs. 4 and 6, we find that for κ_1 to be 0 at this temperature, $M = -0.90$. This value is close to the value of M = -0.83 ± 0.1 estimated in Siegel and Kozlov (4). It will also turn out that the fitted value of M for DOPE-Me is within 0.6% of this value (see below).

Measurement of M and κ_2/k_m for DOPE-Me

From fitting the data in Fig. 1 *A*, we obtain $M = -0.90$ and $\kappa_2/k_m = 2.4$ nm^2. The data seem to follow the functional form in Eq. 7. The standard error of the fit for M is only 0.5%, and the error for κ_2/k_m is 12%. The small variation in M suggests that rather precise measurements of the effects of exogenous lipids and peptides can be made using this method, when one compares c_{eq} for systems containing minor mole fractions of the exogenous substances with c_{eq} for the host lipid. The data in Fig. 1 *A* are obtained between 55 and 90.3°C. One might expect the elastic constants to change over a temperature interval of this size. Thus it is interesting that if one fits only the data between 55 and 65°C, one obtains the same values of κ_2/k_m and M, to within 1% and <0.1%, respectively. This implies that the values of M and κ_2/k_m are nearly constant

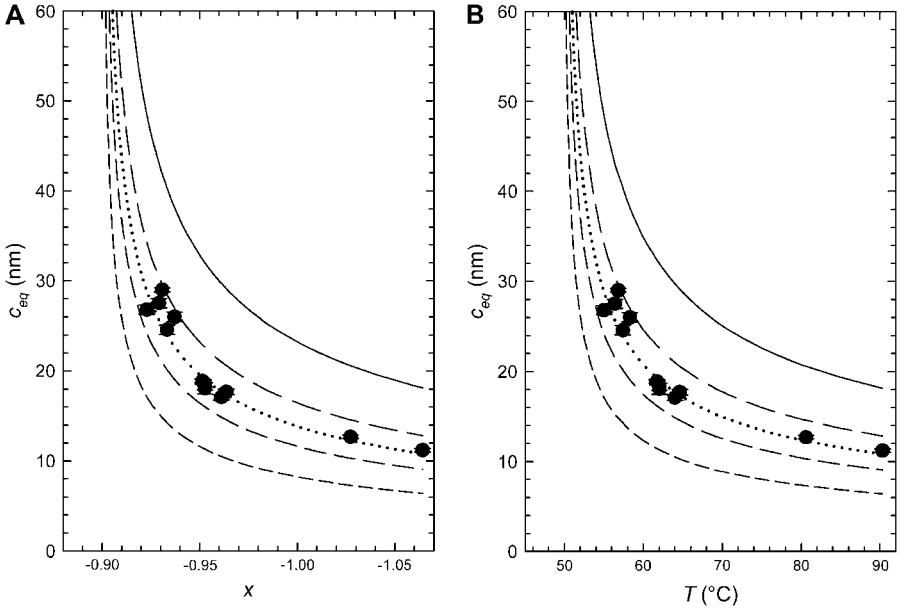

FIGURE 1 (*A*) Plot of theoretical value of c_{eq} versus x (Eq. A18) for Q_{II}-*Pn3m* for DOPE-Me with a value of $M = -0.9$, as estimated in the text, using data in Siegel and Kozlov (4) and Cherezov et al. (5). (*B*) The value c_{eq} versus temperature. The dashed curves are for different assumed values of κ_2/k_m. From top to bottom, the values of κ_2/k_m are $4\delta^2$, 2δ,^{2} δ ^{2}, and $\delta^2/2$. The data points are for DOPE-Me, from Cherezov et al. (5). The dotted curve is the fit to the DOPE-Me data using Eq. 7. The fitted values of the constants in Eqs. 7 and 8 are $M = -0.901 \pm 0.004$ and $\kappa_2/k_m = 2.44 \pm 0.29$ nm^2.

over this interval. This is probably true because M and κ_2/k_m are both ratios of elastic moduli, and the temperature-dependent change in each modulus tends to compensate that of the other.

The fitted value of M can be used to calculate the value of J_s at which $\kappa_1 = 0$ (Eqs. 4–6), and thus to determine the temperature T_K that corresponds to this value. This yields $T_K = 50°C$. Fusion pores are also structures that have $K < 0$ (4). The value $T_K = 50°C$ is compatible with the observation of numerous fusion pores in multilamellar samples incubated at temperatures in this range, and at temperatures at least several degrees below the temperature at which Q_{II} phase is first observed (reviewed in (4,5)). The correspondence of the observed and predicted T_K is another reason for confidence that the functional form of Eq. 7 is correct. At least for data of this quality, it seems that only terms in K and K^2 (S_1 and S_2) in Eq. A17 are sufficient to explain the observed behavior of c_{eq}.

To achieve optimal accuracy in moduli determination from this sort of data, four experimental measures should be taken:

First, it is important that the values of c_{eq} be obtained using samples with a water content in excess of the water content of the equilibrium Q_{II} phase, so that c is not constrained to a smaller, nonequilibrium value. Otherwise, either the Q_{II} phase will not be free to swell so that $c = c_{eq}$, or only part of the sample will be able to enter the Q_{II} phase, leaving some lipid in phases of lower water content (L_α or H_{II}). The water content of a Q_{II} lattice can be estimated from the following equation, where l is the full thickness of the lipid monolayers:

$$\phi_w = 1 - [2A^*(l/c) - 8\pi(l/c)^3/3]. \quad (9)$$

For example, if the total thickness of the lipid monolayers is 1.9 nm, then a Q_{II}-*Pn3m* phase with $c = 40$ nm would have a water content of 82% by volume (7). Even larger values of c have been observed in phospholipid systems ((10); B. Tenchov, R. C. MacDonald, and D. P. Siegel, unpublished). Some of the data in Cherezov et al. (5) may have been obtained with insufficient water content to permit the Q_{II} phase to swell so that $c = c_{eq}$. The accuracy of the fit in Fig. 1 *A* is limited by the scatter in the data, and the scatter is greatest for points with $c > 24$ nm. The water content of the samples used to obtain these data was ~70% (wt) (5). This is less than the equilibrium water content of DOPE-Me Q_{II}-*Pn3m* phases with $c_{eq} > 24$ nm. Thus, some of the scatter may be due to small differences in water content between samples. This emphasizes the importance of using high water contents (~90%). The samples should also be thoroughly equilibrated with the water by numerous freeze/thaw cycles, using a protocol similar to the one in Cherezov et al. (5).

Second, data should be obtained over a broad range of temperatures $> T_K$ starting as close as possible to T_K. The consistency of the fit across the temperature interval should be checked. The values of c_{eq} might be >40 nm at T within several Kelvin of T_K (Fig. 1 *B*). An appropriate detector placement, aperture and resolution should be employed.

Third, δ should also be measured, even if one is comparing the values of M for a host lipid with and without a low mole fraction of exogenous substance. The values M and x depend on δ (Eqs. 5 and 6). Exogenous substances such as membrane-spanning peptides (14) could change T_K and the fitted value of M by changing δ, as well as by changing J_s and k_m. (It is unlikely that δ, M, k_m, and J_s can be changed independently, because they all affect or arise from the monolayer stress profile.) Some membrane-associated peptides can change the average bilayer thickness of a host lipid by as much as 4% at a peptide/lipid ratio of 1:100 mol/mole (17). If a peptide decreased δ by a similar fraction in DOPE-Me, this would decrease the value of x at all J_s. For the purposes of illustration we assume that M, J_s, and κ_2 are all unchanged by the addition of an exogenous peptide, but that the peptide decreases δ by 4%. This change in δ would make the value of J_s needed to make $\kappa_1 = 0$ more negative, and increase T_K by almost 9 K. If one measured the apparent value of M from a plot like Fig. 1 *A*, and assumed the peptide had no effect on δ, one would underestimate the true value of M in the presence of the peptide by ~4%. Therefore, for maximum accuracy in determining M, one should measure δ of the host lipid and of the host lipid/exogenous substance mixtures. This can be done via x-ray diffraction measurements on the L_α phases (17,18).

Fourth, the present treatment assumes that δ is independent of temperature. However, δ may also be temperature-dependent. For example, the bilayer thickness of phosphatidylethanolamines decreases as a function of increasing temperature. For DOPE, it decreases at a rate of ~1.3% for every 10 Kelvin increase in temperature near its L_α/H_{II} phase transition temperature (Fig. 10 of (19)). If δ, the bilayer midplane-to-neutral plane distance, has the same temperature dependence, this will affect the value of κ_2/k_m obtained from a fit of c_{eq} versus x. For purposes of illustration, let us assume that, in DOPE-Me, δ decreases with increasing temperature at the same rate as the total bilayer thickness does in DOPE. Including this affect in the temperature-dependence of x (Eq. 6), refitting the DOPE-Me c_{eq} data in Fig. 1 *A* results in a value of κ_2/k_m that is half as large as the value obtained from the fit assuming that δ is constant, although M is unchanged. Hence, the present treatment tends to overestimate κ_2/k_m. Ideally, one should estimate the temperature dependence of δ and incorporate this dependence into the value of $x(T)$.

DOPE-Me is a convenient host lipid system because it is one of very few single lipid-component lipid systems that spontaneously form the Q_{II} phase. In multicomponent lipid systems, the lipid components may distribute differently between coexisting L_α and Q_{II} phases, and this distribution may change as a function of temperature. This complicates calculation of J_s as a function of temperature. In addition, T_K and T_Q lie in an easily accessible range for DOPE-Me.

In general, experiments should be done in the heating direction. When Q_{II} phases form at high temperatures, there are more Q_{II} phase unit cells per unit area of bilayer than at lower temperatures. If a Q_{II} phase formed at a high temperature is subsequently cooled to a lower temperature, there may not be enough bilayer area to allow all the unit cells to swell to the equilibrium size, c_{eq}. Destruction of Q_{II} phase can be a slow process, since metastable Q_{II} phases formed on cooling below T_Q persist for very long times.

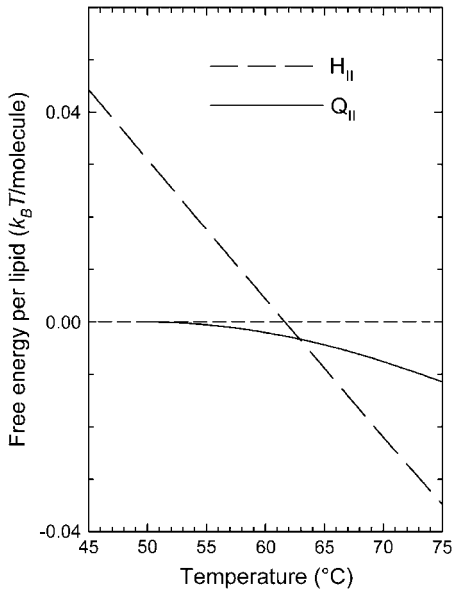

FIGURE 2 Plot of the free energy per molecule of lipid in the Q_{II}-*Pn3m* phase (Eq. 10) and the H_{II} plotted (Eq. 11) in DOPE-Me as a function of temperature. The Q_{II} phase is the equilibrium phase between ~50°C and 63°C.

Implications for Q_{II} phase stability

With Eqs. 1, 7, and 8, it can be shown that

$$\mu_Q = \frac{a}{2}\frac{S_1^2}{S_2 S_0}\left(\frac{-\kappa_1^2}{4\kappa_2}\right), \tag{10}$$

where μ_Q is the free energy per lipid molecule of the Q_{II} phase relative to planar bilayers of the same composition, and a is the area per lipid molecule at the neutral surfaces of the monolayers. Eq. 10 is a relatively simple expression for the free energy of the Q_{II} phase that depends only on observable quantities. It is valid at $T \geq T_K$ for systems in excess water, with $c > 12$ nm (Appendix A). For comparison, the free energy per lipid molecule in the H_{II} phase is (4)

$$\mu_H = \frac{ak_m}{2}[(J_s(T_H))^2 - (J_s(T))^2], \tag{11}$$

where $J_s(T_H)$ is the value of J_s at $T=T_H$, the temperature of the equilibrium L_α/H_{II} phase transition temperature. Eqs. 10 and 11 are plotted as a function of temperature in Fig. 2. This plot reproduces most features of the observed phase behavior in DOPE-Me (5) near the lamellar/inverted phase boundary. In particular, there is a short band of temperatures above T_Q for which H_{II} phase is metastable with respect to Q_{II} phase between ~50°C and 63°C, in agreement with observations (5).

However, Eq. 10 cannot be exact. S_1^2/S_2S_0 has the same value for all bicontinuous Q_{II} phases based on the D, P, or G surfaces of Schoen (16), and is equal to ~0.820545 (3). Hence, Eq. 10 cannot be used to explain why any one of these phases is preferred over the others in the presence of excess water. Yet Q_{II}-*Ia3d* (G) is seldom observed in excess water systems. This degeneracy is probably broken by small differences in the contributions of higher-order terms (K^3 and K^4) in Eq. A17, differences in free energy due to variations in bilayer thickness across the unit cell (3), or by other factors, such as differences in interbilayer interactions within the Q_{II} phase unit cell. In Cherezov et al. (5), it was also observed that whereas H_{II} phase was clearly an equilibrium phase at $T > 66$°C, some Q_{II} phase coexisted with H_{II} at 80–90°C: this is not predicted by the model in Fig. 2. The same values of M and κ_2/k_m are obtained from fits of c_{eq} data in the ranges 55–65°C and 55–90°C. This implies that the same free energy expression applies throughout the 55–90°C interval, so the discrepancy does not seem to be due to a failure in the model for the free energy of the Q_{II} phase. The Q_{II} phase observed in Cherezov et al. (5) at 80–90°C may not be an equilibrium phase. In this regard, it should be noted that the samples in Cherezov et al. (5) were always incubated for 1 h at 55°C before temperature-jumps. Fusion pores and Q_{II} phases are extremely hysteretic: it may be that fusion pores formed during the pore-incubation period later formed Q_{II} phase when driven together by the rapid and extensive formation of H_{II} phase in the high-temperature samples. These measurements should be repeated without the preincubations at lower temperature.

Equation 10 was derived in the large-c limit, where the area of each monolayer neutral plane in a Q_{II} phase unit cell is the same as the area of bilayer midplane. In fact these areas are slightly different (Eq. A3). Formally, the RHS of Eq. 10 should be multiplied by $(1+ \delta^2 \langle K \rangle)$. Using Eqs. A16 and A18, it can be shown that for systems in excess water, this term is identical for *Pn3m*, *Im3m*, and *Ia3d* Q_{II} phases of the same lipid composition at the same value of J_s. For Q_{II} *Pn3m* phases with $c > 15$ nm ($\delta/c < 0.087$), this term decreases the value of μ_Q by less than 5%.

Influence of κ_2/k_m on fusion pore energies and dynamics

When two membrane-bounded vesicles are opposed, the first structure that allows nonleaky communication of the aqueous contents and membrane mixing of the two vesicles is a fusion pore or interlamellar attachment (ILA (20)). These structures are also Q_{II} phase precursors (4,21). As in Siegel and Kozlov (4), it is assumed that the bilayer midplanes of the fusion pore lie on a catenoid (a minimal surface with bilayer curvature $J = 0$). The pore must be distorted from catenoidal geometry at radii far away form the pore axis to merge with the planar bilayers at its periphery (referred to here as a rim). As discussed in Siegel and Kozlov (4), if the rim is joined to the catenoid at distances sufficiently far away from the axis, the curvature energies of these rim regions are $<k_BT$. No such rims are necessary for fusion pore formation between opposed, convexly-curved surfaces, as in exocytosis or many other intracellular fusion events. An equation analogous to Eq. 1 can be written for the curvature free energy of a catenoidal fusion pore:

$$F_{\text{pore}} = \kappa_1 \int_{\text{pore}} KdA + \kappa_2 \int_{\text{pore}} K^2 dA. \qquad (12)$$

The integral $\int KdA$ is $= -4\pi$ (4). In Appendix B it is shown that in physically relevant cases the integral in K^2 reaches a limiting value given by

$$\int_{\text{ILA}} K^2 dA = \frac{4\pi}{r_0^2}\left(\frac{8}{15}\right), \qquad (13)$$

where r_0 is the minimum radius of the pore in the plane perpendicular to the pore axis, evaluated at the bilayer midplanes. The $\int K^2 dA$ term introduces the pore size into the free energy expression (Eq. 11). In contrast, in Siegel and Kozlov, the free energy of a fusion pore was calculated using only the first term on the right-hand side of Eq. 1, which does not depend on pore dimensions (4).

To show the effects of different values of κ_2/k_m on fusion energy and size, F_{pore} is plotted in Fig. 3 for DOPE-Me at 55°C with the same range of values of κ_2/k_m as in Fig. 1. In Fig. 4, F_{pore} is plotted at temperatures $\sim T_Q$ for DOPE-Me, using the value of $\kappa_2/k_m = 2.4\ \text{nm}^2$ determined from the fit in Fig. 1 *A*. Formation of fusion pores at $T < T_K$ can take a substantial amount of energy (e.g., $>17\ k_BT$ at 35°C; Fig. 4). Fusion pores are unstable at small values of r_0, and there is a shallow energy gradient driving pore-widening. However, this gradient is modest: the difference between the values of F_{pore} at $r_0 = 4$ nm and $r_0 = \infty$ is only 1–2.5 k_BT for this range of κ_2/k_m values. This has implications for biomembrane fusion mechanisms. The diameters of nascent fusion pores may be constrained by the sizes of the fusion intermediates and of the fusion-mediating proteins. The driving force for pore expansion that is calculated here is so small that if fusion machines in biomembranes produce fusion pores under conditions where they are not thermodynamically stable, the pores may not have a chance to expand before they revert to the precursor structure. This is consistent with the fact that an important role of viral fusion proteins seems to be to drive expansion of the nascent pore to larger diameters where it is at least kinetically stable or metastable (22,23).

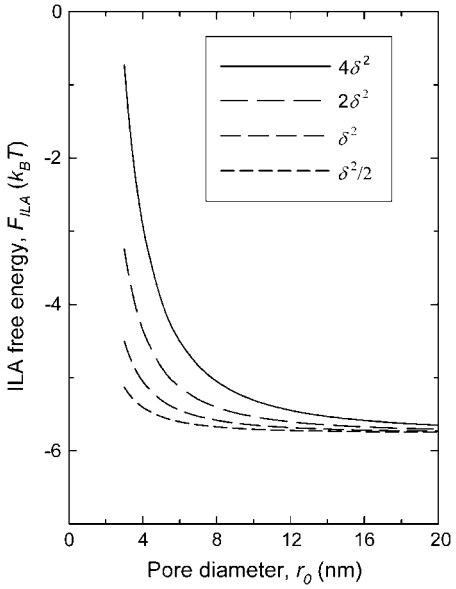

FIGURE 3 Plot of the predicted free energy of a fusion pore in DOPE-Me, F_{pore}, against the radius of the pore at the narrowest point, r_0, for different assumed values of κ_2/k_m. From top to bottom, the curves are plotted with $\kappa_2/k_m = 4\delta^2$, $2\delta^2$, δ^2, and $\delta^2/2$.

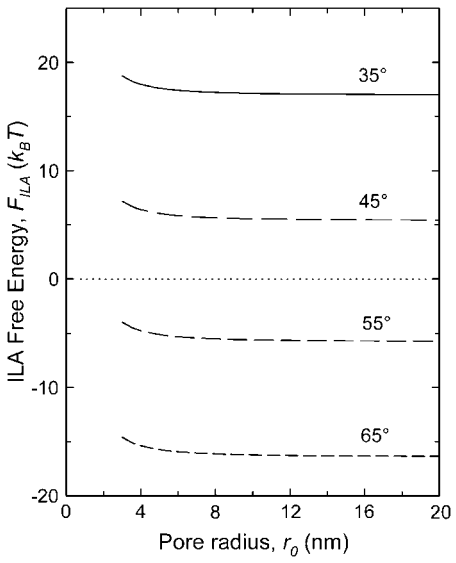

FIGURE 4 Plot of the predicted free energy of a fusion pore in DOPE-Me, F_{pore}, against the radius of the pore at the narrowest point, r_0, at different temperatures. The values are calculated using the value of κ_2/k_m obtained from the fit to the data in Fig. 2.

Biomembrane fusion can occur very rapidly at temperatures near 37°C. The high energy of fusion pores near this temperature in Fig. 4 might give the impression that the stability of these pores is irrelevant to biomembrane processes. It should be noted that the energies in Fig. 4 are for lipids with the properties of DOPE-Me, which has $T_K \approx$ 50°C. (Fig. 1 *B*). Fusion pore formation is spontaneous at $T > T_K$. The value of T_K for mixtures of biomembrane-relevant lipids can lie in the physiological range, and thus formation of fusion pores would be favored when biomembranes of those compositions are apposed under physiological conditions. For example, multilamellar dispersions of DOPC/DOPE/cholesterol (1/1/1, mol/mol/mol) (24) and egg PC/egg PE/cholesterol/diacylglycerol (2/1/1/0.1, mol/mol/mol/mol) (25) form prominent isotropic ^{31}P NMR resonances at 37–40°C, which indicates the spontaneous formation of fusion pores and (possibly) Q_{II} phases. In Nieva et al. (25), it was also shown that vesicles with these lipid compositions fuse rapidly at the same temperatures, and that the fusion rate is correlated with proximity to the L_α/Q_{II} phase boundary. Furthermore, peptides representing parts of fusion-mediating proteins can depress T_K and T_Q relative to the values for the peptide-free lipids (see Conclusions, below).

Implications for the mechanism of the L_α/Q_{II} phase transition

During the L_α/Q_{II} phase transition, fusion pores collect into arrays to form Q_{II} phases at $T > T_Q$ (4,20,21,26); a process driven by the high area density of Gaussian curvature in Q_{II} phases. As more and more fusion pores form in an array of planar bilayers, they automatically form a square lattice with the same topology as the Q_{II}-*Im3m* phase (5,20). More recently, Squires et al. (26) have suggested that there is a direct route between an array of pores and Q_{II}-*Pn3m*. Conn et al. (27) have recently observed evidence of intermediate structures in L_α/Q_{II} transitions via time-resolved x-ray diffraction. These may be the postulated ILA array intermediates.

In fact, at least two infinite periodic minimal surfaces exist that resemble lattices of fusion pores forming within a multilamellar lattice. Interestingly, the number of ILAs per unit of bilayer area in the unit cell is different for the two structures, and the geometries of the two structures suggest an interconversion of the two as the number density of fusion pores in the arrays increase. The first such surface, with the lower density of fusion pores, is one parameterization of the *o-CLP* surface found by Schoen (16) and depicted by Mackay (28). The *o-CLP* structure is depicted in the top part of Fig. 5. As noted by Mackay (28), this structure ''shows the way in which catenoidal bridges may connect almost parallel sheets as perhaps in the transformation of a layer-structured lipid to a cubically-connected structure.'' The second such structure is a family of infinite periodic minimal surfaces that closely resembles the lattice of fusion pores suggested in Cherezov et al. (5) and Siegel (20). A member

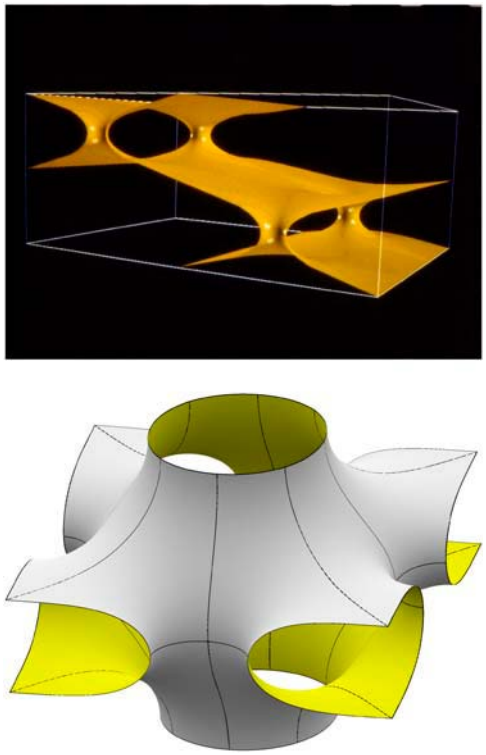

FIGURE 5 (*Top*) One parameterization of the *o-CLP* surface of Schoen (16). If the lipid bilayer midplane resides on the surface, it resembles an array of fusion pores forming between distorted planar bilayers, with the catenoidal elements being the fusion pores. The front surface of the cell outlined by white lines is a cross section containing the vertical axes of two of the catenoidal elements. Illustration from Mackay (28), reproduced with permission. (*Bottom*) A member of the S'-S'' family of minimal surfaces identified in Schoen (16), which may also be an intermediate in the L_α/Q_{II} phase transition. The bilayer midplane lies on the depicted surface. The axes of the component fusion pores are the axis of the entire structure and the axes of the half-pores on the four sides of the structure. Illustration from Brakke (29), used with permission.

of this S'-S'' family (16), as illustrated by Brakke (29), is shown in the bottom part of Fig. 5. This structure would arise from square planar arrays of fusion pores in a multilayer stack of planar bilayers (the axes of the component pores are the axis running down the center of the structure and the axes of half-pores seen on the four sides of the structure). As fusion pores first form within a multilamellar array, they must have rims with nonzero bending elastic energy (4,30). The lowest-energy rims occur when the catenoid extends to radii that are tens or more multiples of r_0 (30), and have curvature energies $<k_BT$ (30,31). Pores can lower their curvature energy (eliminate the rims) by aggregating so as to form minimal surface structures like the *o-CLP* and S'-S'' structures. Such structures may form in sequence during the L_α/Q_{II} phase transition as the number of pores increases in a multilamellar stack. The dimensions of the initial lattices should reflect the dimensions of the pores from which they assemble, and hence the value of r_0. Two adjoining layers of pore-connected lamellae are required to form the nascent Q_{II}

phase-unit cell (5,20,26). How big will these precursor lattices be?

The value of F_{pore} changes very slowly with r_0 for $r_0 > 6$ nm (Figs. 3 and 4). Using the value of κ_2 measured here for DOPE-Me, F_{pore} is only about one-half k_BT larger at $r_0 = 6$ nm than for $r_0 = \infty$. Thus, r_0 will be generally be ≥ 6 nm, but probably not much larger. Since 90% of the favorable Gaussian curvature energy of a fusion pore is contained within a radius = 2.3 r_0 (Appendix B), it is unlikely that the radius of the catenoidal elements of the fusion pore array will be much smaller than 2.3 r_0. At this radius, the height of the pore is ~3 r_0, or ~18 nm. Hence, the initial lattice constant for a structure like the pore array in Cherezov et al. (5) and Siegel (20) would be ≈36 nm. A similar size is estimated for an S'-S'' surface-based structure: if the radii of the smaller channels in the S'-S'' surface are the same size as in the pores from which they assemble, the structure in Fig. 5 would be ~8 r_0 wide and nearly 6 r_0 tall, which leads to an estimated initial value of c of 36–48 nm. For DOPE-Me, these values are comparable to the largest values of c_{eq} observed for DOPE-Me near T_Q, and considerably larger than values of c_{eq} at higher temperatures (Fig. 1 *B*). The nascent Q_{II} lattice can reduce its energy by shrinking in size, which increases the area density of Gaussian curvature. This may explain the curious observation that, after temperature jumps to a constant temperature, nascent Q_{II} lattices tend to shrink with increasing time when they are first developing (5).

The large initial water content of a multilamellar array with a large number of fusion pores may also rationalize the curious effects of different solutes on the kinetics of Q_{II} lattice formation from the L_α phase (10). The local water content of a multilamellar lattice containing fusion pores is very large, because of the large local separation between the bilayers imposed by the pores. Using the parameters estimated in the previous paragraph, the water content is ~80%. Differences in solute composition that reduce long-range attractive forces between planar bilayers, and hence encourage expansion of the lamellar lattice, probably lower the energetic barriers to pore formation, and increase the rate at which they can aggregate laterally within the lamellar array.

CONCLUSIONS

The values M and κ_2/k_m can be determined by x-ray diffraction studies of the Q_{II} phase in excess water at $T > T_Q$. It should be possible to determine the effects of small mole fractions of peptides and exogenous lipids on M of a host lipid to within a few percent. It has been suggested (13) that the moieties of fusion-mediating proteins act in part by increasing the value of κ, since this elastic modulus has substantial effects on the energy needed to create fusion intermediates (11). The value of κ also determines the stability of the fusion pore itself (i.e., κ can determine whether there is a net driving force for membrane fusion under given circumstances (4)). Because of their role in protein-catalyzed membrane fusion, fusion peptides and transmembrane domains of fusion-mediating proteins would be excellent candidates for such studies. Fusion peptides have long been known to lower T_K and lower the temperature at which fusion occurs in lipid systems (reviewed in (13)), and as noted in Theoretical Results, reductions in T_K most likely correspond to increases in M. It has also been shown that membrane-spanning peptides lower the temperature at which Q_{II} phases form (T_Q) (14). Accordingly, the membrane-spanning peptides of viral fusion proteins have been shown to induce liposome fusion in systems containing no other proteins (32–35).

The analysis also shows (Eqs. 5 and 6) that membrane-associated peptides can affect fusion pore and Q_{II} phase stability through small effects on δ, which can accompany changes in bilayer thickness. This may explain some of the Q_{II}-phase stabilizing features of membrane-spanning peptides, and perhaps some features of what has been called the hydrophobic mismatch effect in Q_{II} phases (e.g., (14, 36–38)). Peptides that increase δ, if they had no effect on M, would increase (make less negative) the value of J_s required to make $\kappa_1 = 0$ (Eq. 6). This would, in turn, decrease the apparent T_Q relative to that of the pure host lipid. Thus, it is possible that this is one factor underlying the curious ability of membrane-spanning peptides that are longer than the host lipid bilayer thickness to decrease T_Q (14,38).

To our knowledge, the present technique is the first experimental method for measuring the contributions of higher-order elastic terms (initially, κ_2/k_m) to the stability of Q_{II} phases and fusion pores. For Q_{II} phases, the analysis also results in a simple form for the free energy of the Q_{II} phase versus the L_α phase in excess water, based only on measurable quantities (Eq. 10). This relationship, and knowledge of higher-order curvature effects, may prove useful in understanding the stability of other inverted phases, and of curved membrane structures in biomembranes like fusion intermediates, fission intermediates, and organelles of complex topology (12,39,40).

APPENDIX A

The midplanes of the bilayer lie on a surface whose curvature J at any point = $1/R_1 + 1/R_2$ and whose Gaussian curvature $K = 1/R_1R_2$, where R_1 and R_2 are the principal radii of curvature of the surface at the given point. Both monolayers of the bilayer are assumed to be identical in composition, and the neutral plane of the monolayers lies a constant distance δ from the bilayer midplanes. The spontaneous curvature of the lipid is J_s. The monolayer curvature and Gaussian curvature evaluated at the neutral surfaces are J_{in} and J_{out}, and K_{in} and K_{out}, respectively, for the two monolayers of the bilayer. The area of the bilayer midplanes is A, and those of the two monolayers are A_{in} and A_{out}. For catenoidal fusion pores and bicontinuous Q_{II} phases, the bilayer midplane lies on a minimal surface, where $J = 0$. As in Siegel and Kozlov (4) and Shemesh et al. (39), the curvature and Gaussian curvature of the monolayers can be expressed in terms of the curvature and Gaussian curvature of the bilayer midplanes:

$$J_{out} = J_{in} = \frac{2\delta K}{1 + \delta^2 K}, \tag{A1}$$

$$K_{out} = K_{in} = \frac{K}{1+\delta^2 K}, \tag{A2}$$

$$A_{out} = A_{in} = A(1+\delta^2 K). \tag{A3}$$

The bending energy of the monolayers to fourth-order in curvature is given by (39)

$$f_i = A_i\left(\frac{k_m}{2}(J_i - J_s)^2 + \kappa K_i + f_3 + f_4\right), \tag{A4}$$

where the subscript i indicates the monolayer identity (inner or outer). The values k_m and κ are the monolayer bending modulus and Gaussian (saddle splay) curvature moduli; respectively. The values f_3 and f_4 are the terms that are third- and fourth-order in monolayer curvature, respectively (39,41):

$$f_3 + f_4 = \eta_1 J_i^3 + \eta_2 J_i K_i + \eta_3 J_i^4 + \eta_4 J_i^2 K_i + \bar{\bar{\kappa}} K_i^2. \tag{A5}$$

The coefficients η_j and $\bar{\bar{\kappa}}$ are unknown. The free energy of the bilayer per unit area ($A = 1$ in Eq. A3) is

$$f_B = (1+\delta^2 K)(f_{in} + f_{out}). \tag{A6}$$

By substituting Eqs. A1–A3 into Eqs. A4–A6, f_B becomes

$$\begin{aligned} f_B = {} & \{2\kappa - 4\delta k_m J_s + \delta^2 k_m J_s^2\}[K] + \{4\delta^2 k_m + 4\delta\eta_2 + 2\bar{\bar{\kappa}}\} \\ & \times\left[\frac{K^2}{1+\delta^2 K}\right] + \{16\delta^3\eta_1 + 8\delta^2\eta_4\}\left[\frac{K^3}{(1+\delta^2 K)^2}\right] \\ & + \{32\delta^4\eta_3\}\left[\frac{K^4}{(1+\delta^2 K)^3}\right]. \end{aligned} \tag{A7}$$

In Eqs. A4 and A5, we have expressed the monolayer curvature energy in terms of monolayer curvature up to the fourth order (e.g., J_i^2, K_i, J_i^3, $J_i^2 K_i$, J_i^4, K_i^2). On minimal-surface-based structures, the monolayer curvatures J_i and K_i are both proportional to K when expressed in terms of curvature at the bilayer midplane (Eqs. A1 and A2). Hence, to make Eq. A7 consistent with our choice of considering only terms up to fourth-order in monolayer curvature (Eq. A4), we should retain terms up to K^4 in Eq. A7. Thus, we express the terms containing K^2, K^3, and K^4 in Eq. A7 as series expansions, and retain only terms up to K^4 in the results:

$$\frac{K^2}{1+\delta^2 K} \approx K^2(1 - \delta^2 K + \delta^4 K^2) = K^2 - \delta^2 K^3 + \delta^4 K^4, \tag{A8}$$

$$\begin{aligned} \frac{K^3}{(1+\delta^2 K)^2} = \frac{K^3}{1+2\delta^2 K+\delta^4 K^2} &\approx K^3(1-2\delta^2 K) \\ &= K^3 - 2\delta^2 K^4, \end{aligned} \tag{A9}$$

$$\frac{K^4}{(1+\delta^2 K)^3} = \frac{K^4}{(1+3\delta^2 K+3\delta^4 K^2+\delta^6 K^3)} \approx K^4. \tag{A10}$$

Substituting these expressions into Eq. A7 yields

$$f_B = \kappa_1 K + \kappa_2 K^2 + \kappa_3 K^3 + \kappa_4 K^4, \tag{A11}$$

where

$$\kappa_1 = 2\kappa - 4\delta k_m J_s + \delta^2 k_m J_s^2 \tag{A12}$$

$$\kappa_2 = 4\delta^2 k_m + 4\delta\eta_2 + 2\bar{\bar{\kappa}} \tag{A13}$$

$$\kappa_3 = 16\delta^3\eta_1 + 8\delta^2\eta_4 - \delta^2\kappa_2 \tag{A14}$$

$$\kappa_4 = 32\delta^4\eta_3 + \delta^4\kappa_2 - 2\delta^2\kappa_3. \tag{A15}$$

The area average of Eq. A11 is the energy per unit area of bilayer in the Q_{II} phase. The integrals of K^N over a unit cell of the Q_{II} phase for values of N up to 8 have been calculated (3,8) in terms of c, the length of the side of the cubic unit cell. The integrals were calculated in the form

$$\int K^N dA = \frac{1}{c^{2N-2}} S_N, \tag{A16}$$

where the values of the coefficients S_N are dimensionless constants, and have different values for the Q_{II} phases corresponding to different infinite periodic minimal surfaces, i.e., *Im3m*, *Pn3m*, *Ia3d*, based on the P, D, and G surfaces of Schoen (16). Note that the values for *Pn3m* in Schwarz and Gompper (3) are for a unit cell twice as large as for the values in Anderson et al. (8). The values in Anderson et al. (8) are appropriate for analysis of x-ray data from Q_{II} phases composed of bilayers without sidedness. Values for the three commonly-observed bicontinuous Q_{II} phases are given in Table 1. The area of the membrane in a unit cell of Q_{II} phase is $S_0 c^2$, and the area average $\int K^N dA/A$ is $S_N c^{-(2N-2)}/S_0 c^2 = S_N/S_0 c^{2N}$. Thus, the area average of Eq. A11 over the unit cell is given by

$$\begin{aligned} f_B = {} & \kappa_1\left[\frac{S_1}{S_0}\right]\left(\frac{1}{c^2}\right) + \kappa_2\left[\frac{S_2}{S_0}\right]\left(\frac{1}{c^4}\right) + \kappa_3\left[\frac{S_3}{S_0}\right]\left(\frac{1}{c^6}\right) \\ & + \kappa_4\left[\frac{S_4}{S_0}\right]\left(\frac{1}{c^8}\right). \end{aligned} \tag{A17}$$

The values of the elastic moduli κ_I can be determined from observed values of c as a function of J_s, which is in turn a function of temperature. The value of c that minimizes the free energy in Eq. A17 in the absence of any restriction on the extent of swelling of the phase will be the equilibrium value of the unit cell constant in excess water, c_{eq}. The value of c_{eq} is found by differentiating Eq. A17 with respect to c, setting the result equal to zero, and rearranging. However, this yields a sixth-order polynomial in c_{eq}. To minimize the number of parameters in fitting observed values of c_{eq}, we wish to test whether using only the first two terms in Eq. A17 (expressing the free energy of the Q_{II} phase bilayer only in terms of K and K^2) generates an adequate fit to the data. Since the values of η_i in Eqs. A13–A15 are in general unknown, the adequacy of this approximation cannot be predicted. However, it can be shown that the approximation for the K^2 term in Eq. A8 is appropriate: using the tabulated values of S_N, it can be shown that the area average of $K^2/(1+\delta^2 K)$ is equal to the area average of K^2 to within 10% for $c > 12$ nm, which is the case for all of the DOPE-Me data used here to test the model. (For most of the data points, $c > 17$ nm, for which the error is $<5\%$.)

Retaining only the first and second terms in Eq. A17 yields a simple expression for c_{eq}:

$$c_{eq} = \sqrt{-\frac{2\kappa_2 S_2}{\kappa_1 S_1}}. \tag{A18}$$

The value S_1 is < 0, and we expect that κ_2 is > 0, since this is necessary to impose an equilibrium value of c in Q_{II} phases. If one uses only the K^1 term in Eq. A17, one obtains the awkward result that the Q_{II} phase should shrink indefinitely (4). The known or estimated values of components of κ_2 (Eq. A13) are consistent with this expectation. The first term on the right-hand side of Eq. A13 is positive. The ratio of this term to k_m is $4\delta^2 = 7$ nm^2, while the ratio of kappa double-bar to k_m is estimated to be ≈ -3 nm^2 (39). This suggests that $0 < \kappa_2/k_m < 7$ nm^2. The value of κ_2/k_m obtained from the data in Fig. 1 *A* for DOPE-Me ($+2.4$ nm^2) is consistent with this. The fitted value of κ_2/k_m also indicates that

$$\frac{2\delta\eta_2 + \bar{\bar{\kappa}}}{k_m} \approx -2 \text{ nm}^2.$$

APPENDIX B

An expression analogous to Eq. A11 can be written for the total energy of a fusion pore with respect to the same area of planar bilayer.

Using the same notation as in the Appendix of Kozlovsky and Kozlov (40), the catenoid is described by

$$\sin(\varphi) = \frac{r_0}{r}, \tag{A19}$$

where r is the radius from the axis, r_0 is the minimum radius of the pore evaluated at the bilayer midplanes, and φ is the tangential angle of the surface profile. Let φ_b be the tangential angle where the catenoid merges with the rim that adapts it to the surrounding planar bilayers. The integral of K^2 over a catenoid that is symmetric across the plane perpendicular to the axis can be shown to be

$$\int_{\text{catenoid}} K^2 dA = -\frac{2\pi}{r_0^2}\int_{\pi-\varphi_b}^{\varphi_b} \sin^5(\varphi)d\varphi = \frac{4\pi}{r_0^2}\left[\frac{\sin^4(\varphi_b)\cos(\varphi_b)}{5} + \frac{4\cos(\varphi_b)\{\sin^2(\varphi_b)+2\}}{15}\right]. \tag{A20}$$

Ninety-nine percent of the value of the integral in Eq. A20 is concentrated within the region $33° < \varphi < 147°$, which corresponds to $r < 1.8\ r_0$. In contrast, the Gaussian curvature of a fusion pore is given by (40)

$$\int_{\text{catenoid}} KdA = -2\pi(\cos(\varphi_b) - \cos(\pi - \varphi_b)) = -4\pi\cos(\varphi_b). \tag{A21}$$

With Eq. A21, it can be shown that 90% of the Gaussian curvature, and hence 90% of the favorable Gaussian curvature energy for pore formation, lies within an area given by $26° < \phi < 154°$, which corresponds to $r < 2.3\ r_0$.

Note added in proof: Equation 10 only expresses the curvature energy difference between the L_α and Q_{II} phases. For better accuracy, Eq. 10 should include a term describing the difference in interbilayer attractive forces in the two phases, as well. The size of this term can determine the value of T_Q relative to T_K and may distort the c_{eq} versus T curve at low temperatures (Fig. 1 *B*). This term is small for lipids like DOPE-Me, but some other lipids have large bilayer-bilayer adhesion energies. Calculations suggest that the measured adhesion energies of phosphatidylethanolamines (PEs), for example, are large enough to make Q_{II} phase unstable (D. P. Siegel, unpublished results), so that μ_Q is either >0 or $>\mu_H$ at all temperatures in excess water. This could explain the absence of spontaneous Q_{II} phase formation when PE systems are heated. The effects of the adhesion energy term on Q_{II} phase behavior will be discussed in a subsequent publication.

The author is very grateful to M. M. Kozlov for illuminating discussions and for comments on a draft of the manuscript.

REFERENCES

1. Helfrich, W., and H. Rennschuh. 1990. Landau theory of the lamellar-to-cubic phase transition. *Coll. Phys. C7 (Fr.)*. 51:189–195.
2. Templer, R. H., B. J. Khoo, and J. M. Seddon. 1998. Gaussian curvature modulus of an amphiphillic monolayer. *Langmuir*. 14:7427–7434.
3. Schwarz, U. S., and G. Gompper. 2001. Bending frustration of lipid-water mesophases based on cubic minimal surfaces. *Langmuir*. 17: 2084–2096.
4. Siegel, D. P., and M. M. Kozlov. The Gaussian curvature elastic modulus of *n*-monomethylated dioleoylphosphatidylethanolamine: relevance to membrane fusion and lipid phase behavior. *Biophys. J*. 87:366–374.
5. Cherezov, V., D. P. Siegel, W. Shaw, S. W. Burgess, and M. Caffrey. 2003. The kinetics of non-lamellar phase formation in DOPE-Me: relevance to biomembrane fusion. *J. Membr. Biol*. 195:165–182.
6. Rand, R. P., N. L. Fuller, S. M. Gruner, and V. A. Parsegian. 1990. Membrane curvature, lipid segregation, and structural transitions for phospholipids under dual-solvent stress. *Biochemistry*. 29:76–87.
7. Schwarz, U. S., and G. Gompper. 2002. Bicontinuous surfaces in self-assembling amphiphillic systems. *Lecture Notes Phys*. 600:107–151.
8. Anderson, D. M., S. M. Gruner, and S. Leibler. 1988. Geometrical aspects of the frustration in the cubic phases of lyotropic liquid crystals. *Proc. Natl. Acad. Sci. USA*. 85:5364–5368.
9. Longley, W., and T. J. McIntosh. 1983. A bicontinuous tetrahedral structure in a liquid-crystalline lipid. *Nature*. 303:612–614.
10. Tenchov, B., R. Koynova, and G. Rapp. 1998. Accelerated formation of cubic phases in phosphatidylethanolamine dispersions. *Biophys. J*. 75:853–866.
11. Kozlovsky, Y., A. Efrat, D. P. Siegel, and M. M. Kozlov. 2004. Stalk phase formation: effects of dehydration and saddle splay modulus. *Biophys. J*. 87:2508–2521.
12. Zimmerberg, J., and M. M. Kozlov. 2006. How proteins produce cellular membrane curvature. *Nat. Rev. Mol. Cell Biol*. 7:9–19.
13. Siegel, D. P. 2005. The relationship between bicontinuous inverted cubic phases and membrane fusion. *In* Bicontinuous Liquid Crystals, Vol. 127 of the Surfactant Science Series. M. L. Lynch and P. T. Spicer, editors. Taylor and Francis, Boca Raton, FL. 59–98.
14. Siegel, D. P., V. Cherezov, D. V. Greathouse, R. E. Koeppe II, J. Antoinette Killian, and M. Caffrey. 2006. Transmembrane peptides stabilize inverted cubic phases in a biphasic length-dependent manner: implications for protein-induced membrane fusion. *Biophys. J*. 90:200–211.
15. Schroth-Diez, B., K. Ludwig, B. Baljinnyam, C. Kozerski, Q. Huang, and A. Hermann. 2000. The role of the transmembrane and of the intraviral domain of glycoproteins in membrane fusion of enveloped viruses. *Biosci. Rep*. 20:571–595.
16. Schoen, A. H. 1970. Infinite periodic minimal surfaces without self-intersections. NASA Technical Note D-5541. National Technical Information Services, Springfield, VA. Document N70–29782.
17. Rand, R. P., and V. A. Parsegian. 1989. Hydration forces between phospholipid bilayers. *Biochim. Biophys. Acta*. 988:351–376.
18. Chen, F. Y., M. T. Lee, and H. W. Huang. 2003. Evidence of membrane thinning effect as the mechanism for peptide-induced pore formation. *Biophys. J*. 84:3751–3758.
19. Harper, P. E., D. A. Mannock, R. N. A. H. Lewis, R. N. McElhaney, and S. M. Gruner. 2001. X-ray diffraction structures of some phosphatidylethanolamine lamellar and inverted hexagonal phases. *Biophys. J*. 81:2693–2706.
20. Siegel, D. P. 1986. Inverted micellar intermediates and the transitions between lamellar, inverted hexagonal, and cubic lipid phases. III. Formation of isotropic and inverted cubic phases and fusion via intermediates in transitions between L_α and H_{II} phases. *Chem. Phys. Lipids*. 42:279–301.
21. Siegel, D. P. 1999. The modified stalk mechanism of lamellar/inverted phase transitions and its implications for membrane fusion. *Biophys. J*. 76:292–313.
22. Schroth-Diez, B., K. Ludwig, B. Baljinnyam, C. Kozerski, Q. Huang, and A. Hermann. 2000. The role of the transmembrane and of the intraviral domain of glycoproteins in membrane fusion of enveloped viruses. *Biosci. Rep*. 20:571–595.
23. Earp, L. J., S. E. Delos, H. E. Park, and J. M. Whie. 2004. The many mechanisms of viral membrane fusion proteins. *Curr. Top. Microbiol. Immunol*. 285:25–66.
24. Tilcock, C. P. S., M. B. Bally, S. B. Farren, and P. R. Cullis. 1982. Influence of cholesterol on the structural preferences of dioleoylphosphatidylethanolamine-dioleoylphosphatidylcholine systems: a phosphorus-31 and deuterium nuclear magnetic resonance study. *Biochemistry*. 21:4596–4601.
25. Nieva, J. L., A. Alonso, G. Basáñez, F. M. Goñi, A. Gulik, R. Vargas, and V. Luzzati. 1995. Topological properties of two cubic phases of a phospholipid:cholesterol:diacylglycerol aqueous system and their possible implications in the phospholipase C-induced liposome fusion. *FEBS Lett*. 368:143–147.

26. Squires, A. M., R. H. Templer, J. M. Seddon, J. Woenckhaus, R. Winter, S. Finet, and N. Theyencheri. 2002. Kinetics and mechanism of the lamellar to gyroid inverse bicontinuous cubic phase transition. *Langmuir*. 18:7384–7392.

27. Conn, C. E., O. Ces, X. Mulet, S. Finet, R. Winter, J. M. Seddon, and R. H. Templer. 2006. Dynamics of structural transformations between lamellar and inverse bicontinuous cubic lyotropic phases. *Phys. Rev. Lett*. 96:108102.

28. Mackay, A. L. 1995. Flexicrystallography: curved surfaces in chemical structures. *Curr. Sci.* 69:151–161.

29. Brakke, K. 2005. http://www.susqu.edu/facstaff/b/brakke/evolver/examples/periodic/ss/sscube.8.gif.

30. Kozlov, M. M., and L. V. Chernomordik. 1998. A mechanism of protein-mediated fusion: coupling between refolding of the influenza hemagglutinin and lipid rearrangements. *Biophys. J*. 75:1384–1396.

31. Petrov, A. G., and M. M. Kozlov. 1984. Curvature elasticity and passage formation in lipid bilayer lattice of passages. *Comptes Rendus Acad. Bulgares Sci*. 37:1191–1194.

32. Langosch, D., B. Brosig, and R. Pipkorn. 2001. Peptide mimetics of the vesicular stomatitis virus G-protein transmembrane segment drive membrane fusion in vitro. *J. Biol. Chem*. 276:32016–32021.

33. Langosch, D., J. M. Crane, B. Brosig, A. Hellwig, L. K. Tamm, and J. Reed. 2001. Peptide mimetics of SNARE transmembrane segments drive membrane fusion depending on their conformational plasticity. *J. Mol. Biol*. 311:709–721.

34. Dennison, S. M., N. Greenfield, J. Lenard, and B. R. Lentz. 2002. VSV transmembrane domain (TMD) peptide promotes PEG-mediated fusion of liposomes in a conformationally sensitive fashion. *Biochemistry*. 41:14925–14934.

35. Hofman, M. W., K. Weise, J. Ollesch, P. Agrawal, H. Stalz, W. Stelzer, F. Hulsbergen, H. de Groot, K. Gerwert, J. Reed, and D. Langosch. 2004. De novo design of conformationally flexible transmembrane peptides driving membrane fusion. *Proc. Natl. Acad. Sci. USA*. 101:14776–14781.

36. van der Wel, P. C. A., T. Pott, S. Morein, D. V. Greathouse, R. E. Koeppe II, and J. A. Killian. 2000. Tryptophan-anchored transmembrane peptides promote formation of nonlamellar phase in phosphatidylethanolamine model membranes in a mismatch-dependent manner. *Biochemistry*. 39:3124–3133.

37. Morein, S., R. E. Koeppe II, G. Lindblom, B. de Kruijff, and J. A. Killian. 2000. The effect of peptide/lipid hydrophobic mismatch on the phase behavior of model membranes mimicking the lipid composition of *Escherichia coli* membranes. *Biophys. J*. 78:2475–2485.

38. Liu, F., R. N. A. H. Lewis, R. S. Hodges, and R. N. McElhaney. 2001. A differential scanning calorimetric and ^{31}P NMR spectroscopic study of the effect of transmembrane peptides on the lamellar-reversed hexagonal phase transition of phosphatidylethanolamine model membranes. *Biochemistry*. 40:760–768.

39. Shemesh, T., A. Luin, V. Malhotra, K. N. J. Boerger, and M. M. Kozlov. 2003. Prefission constriction of Golgi tubular carriers driven by local lipid metabolism: a theoretical model. *Biophys. J*. 85:3813–3827.

40. Kozlovsky, Y., and M. M. Kozlov. 2003. Membrane fission: model for intermediate structures. *Biophys. J*. 85:85–96.

41. Mitov, M. D. 1978. Third and fourth order curvature elasticity of lipid bilayers. *Comptes Rendus Acad. Bulgares Sci*. 31:513–515.